Modeled seasonality of glacial abrupt climate events

Author(s):
Flückiger, Jacqueline; Knutti, Reto; White, James W.C.; Renssen, Hans

Publication date:
2008-11

Permanent link:
https://doi.org/10.3929/ethz-b-000013465

Originally published in:
Climate Dynamics 31(6), https://doi.org/10.1007/s00382-008-0373-y

Clim Dyn (2008) 31:633–645
DOI 10.1007/s00382-008-0373-y

Modeled seasonality of glacial abrupt climate events

Jacqueline Flückiger · Reto Knutti · James W. C. White · Hans Renssen

Received: 8 December 2006 / Accepted: 15 January 2008 / Published online: 9 February 2008

Abstract Greenland ice cores, as well as many other paleo-archives from the northern hemisphere, recorded a series of 25 warm interstadial events, the so-called Dansgaard-Oeschger (D-O) events, during the last glacial period. We use the three-dimensional coupled global ocean–atmosphere–sea ice model ECBILT-CLIO and force it with freshwater input into the North Atlantic to simulate abrupt glacial climate events, which we use as analogues for D-O events. We focus our analysis on the Northern Hemisphere. The simulated events show large differences in the regional and seasonal distribution of the temperature and precipitation changes. While the temperature changes in high northern latitudes and in the North Atlantic region are dominated by winter changes, the largest temperature increases in most other land regions are seen in spring. Smallest changes over land are found during the summer months. Our model simulations also demonstrate that the temperature and precipitation change patterns for different intensifications of the Atlantic meridional overturning circulation are not linear. The extent of the transitions varies, and local non-linearities influence the amplitude of the annual mean response as well as the response in different seasons. Implications for the interpretation of paleo-records are discussed.

Keywords Climate modeling · Dansgaard-Oeschger events · Glacial · Seasonality · Meridional overturning circulation

J. Flückiger · J. W. C. White
Institute of Arctic and Alpine Research, University of Colorado, Campus Box 450, Boulder, CO 80309, USA

J. Flückiger (✉)
Environmental Physics,
Institute of Biogeochemistry and Pollutant Dynamics,
ETH Zürich, Universitätstrasse 16, 8092 Zurich, Switzerland
e-mail: jacqueline.flueckiger@env.ethz.ch

R. Knutti
Institute for Atmospheric and Climate Science,
ETH Zürich, Universitätstrasse 16, 8092 Zurich, Switzerland

H. Renssen
Faculty of Earth and Life Sciences,
Vrije Universiteit Amsterdam, De Boelelaan 1085, 1081 HV Amsterdam, The Netherlands

1 Introduction

The last glacial period was punctuated by 25 warm phases in the northern hemisphere, so called Dansgaard-Oeschger (D-O) events or interstadials. They are seen most prominently in Greenland temperature proxy records measured along Greenland ice cores (Dansgaard et al. 1993; North Greenland Ice Core Project members 2004). Annual mean temperature in Greenland rose by 8–16°C within only a couple of decades at the onset of the events (Huber et al. 2006; Landais et al. 2004; Lang et al. 1999), followed by a gradual cooling over centuries to millennia before the warm periods abruptly ceased. D-O events were not limited to Greenland and the North Atlantic region but are imprinted in paleo-archives in most other regions of the northern hemisphere and even at a few locations in the southern hemisphere (Voelker and workshop participants 2002). They can be detected for example in temperature and precipitation records from Europe (Genty et al. 2003; Müller et al. 2003; Spötl and Mangini 2002), Asia (Ji et al. 2004; Wang et al. 2001), and North America (Zic et al. 2002), in marine cores from the North Atlantic, indicating sea surface temperature

(SST) changes and changes in the strength of the Atlantic meridional overturning circulation (AMOC) (Curry and Oppo 1997; Elliot et al. 2002; McManus et al. 2004; Shackleton et al. 2000), in the Arabian Sea, showing changes in oceanic upwelling associated with changes in monsoon strength (Schulz et al. 1998), in the Cariaco Basin indicating precipitation shifts (Peterson et al. 2000), in the Santa Barbara Basin showing SST and intermediate water temperature changes probably caused by changes in the trade wind strength (Hendy and Kennett 2003), and in Baja California indicating changes in marine productivity (Ortiz et al. 2004). Paleo-records are often influenced by seasonal rather than by annual mean climate and indicate that temperature changes during D-O events are mainly a winter phenomenon at least in the North Atlantic region (Denton et al. 2005; Renssen and Isarin 2001). Therefore, it is essential to study the seasonal signals in modeled abrupt climate events in order to better understand the observed variations in proxy records.

Many model studies have focused on the annual mean behavior of abrupt glacial climate events and were able to explain several important characteristics of these events, such as their extent, aspects of their timing, and the involved feedback mechanisms (Flückiger et al. 2006; Ganopolski and Rahmstorf 2001; Ganopolski and Rahmstorf 2002; Marchal et al. 1998; Schmittner et al. 2003, 2002; Stocker and Marchal 2000). But only few modeling studies have discussed the seasonal characteristics of such events. Most of the publications that have studied seasonality are based on results from atmospheric general circulation models (AGCM) with prescribed SST and sea ice edges or ocean surface heat fluxes. They have focused on climatic changes in Greenland (Fawcett et al. 1997; Li et al. 2005) or Europe and the North Atlantic region (Renssen and Bogaart 2003; Renssen and Isarin 2001). They confirm the strong dominance of winter versus summer temperature changes during abrupt glacial climate events in these areas. Other results are based on a zonally averaged climate model (Schmittner and Stocker 2001) and focus on the stability of the AMOC in a seasonal versus an annual mean version of the model. The results for an AMOC off to on transition in the seasonal model shows the largest zonally averaged temperature changes in late winter to early spring in mid to high northern latitudes.

Our study goes several steps further than the previously published modeling papers discussed above. We use the three-dimensional climate model ECBILT-CLIO, a fully coupled atmosphere–ocean–sea ice model of intermediate complexity to simulate the regional and seasonal responses of the abrupt warming events in the northern hemisphere caused by transitions from weak or halted AMOC states to an AMOC state with a stronger overturning circulation. In contrast to the earlier AGCM studies, the dynamical ocean and sea ice models allow the ocean and sea ice to evolve freely, and we do not have to prescribe SST, sea ice edges or ocean surface heat fluxes. This ensures climate response patterns that are consistent and coupled across the atmosphere, ocean and sea ice components within that model. Further, we are interested in the seasonality of these abrupt events in the whole northern hemisphere instead of focusing only on the North Atlantic and European regions.

The following section of this paper describes the model and the experiments performed (Sect. 2). Section 3 explores different oceanic equilibrium states and transitions between the different states; Sect. 4 discusses the atmospheric responses in different seasons to an AMOC change and Sect. 5 shows implications of our modeling results on the interpretation of paleo-records measured along different archives.

2 Model setup, experiments and evaluation

ECBILT-CLIO version 3 is a global, coupled atmosphere–ocean–sea ice model. The atmosphere is represented by the T21, 3-level quasi-geostrophic model ECBILT (Opsteegh et al. 1998), which contains a full hydrological cycle and explicitly computes synoptic variability associated with weather patterns. The ocean model CLIO is a primitive equation, free-surface ocean general circulation model with a resolution of three by three degrees and 20 unevenly spaced depths layers, coupled to a thermodynamic, dynamic sea ice model (Goosse and Fichefet 1999). The coupled atmosphere–ocean model includes realistic topography and bathymetry, a simple representation of land surface processes and a bucket-style freshwater runoff scheme. It incorporates weak freshwater flux corrections. The precipitation over the Atlantic and Arctic basins is reduced by 8.5 and 25%, respectively, and homogeneously redistributed over the North Pacific. The model and a complete list of references are available at the web site http://www.knmi.nl/onderzk/CKO/ecbilt.html.

The simulations presented in this paper use boundary conditions of the last glacial maximum (LGM) for greenhouse gas concentrations, orbital parameters, topography on land and albedo values (Timmermann et al. 2004). Besides these modifications in the boundary conditions no attempt was made to tune ECBILT-CLIO towards a specific behavior or equilibrium state. The resulting glacial control run shows a strong AMOC with a maximum in the North Atlantic of 24.9 Sv compared to 26.1 in the preindustrial control run. The maximum North Atlantic deep water (NADW) export at 30°S is slightly stronger than in the preindustrial control run (17.1 versus 15.1 Sv). We do

not consider this climate state as an analogue for the LGM state since paleo-data indicate a weaker and shallower AMOC during the LGM compared to preindustrial (Lynch-Stieglitz et al. 2007; Sarnthein et al. 2000). Instead the glacial control run is used as an analogue for the warm interstadial phases of the last glacial period. A LGM state with a weaker AMOC can be obtained by forcing the model with a positive freshwater anomaly in the North Atlantic. Applying a freshwater forcing to get to an LGM state might seem to be in contradiction with paleo-data. However, since ECBILT-CLIO uses freshwater flux corrections the zero line of freshwater forcing in the North Atlantic is actually unknown. Also, a small background freshwater flux from the northern hemisphere ice sheets is probably a reasonable assumption for the whole glacial period. This was not taken into account in our model setup. No further attempt is made here to simulate an LGM state as realistic as possible since this is not the focus of the paper and can be found elsewhere (Roche et al. 2007).

Freshwater input, prescribed as a step function into the whole North Atlantic between 50°N and 70°N is used to force a reduction in the AMOC (Fig. 1). After decreasing the freshwater forcing to zero, the ocean circulation recovers within decades to a few centuries to the strength of the glacial control run that has no freshwater forcing applied. In contrast to earlier studies (Flückiger et al. 2006; Knutti et al. 2004) the freshwater input is not compensated, therefore, the average salinity of the global oceans is not constant over time. We use the average over the model years 4,600–4,800 of the freshwater forced runs as analogs for the cold, stadial climate states with reduced or halted AMOC, and the glacial control run, as an analog for a warm interstadial phase (see discussion above). In particular we use the differences between the glacial control run (called strong AMOC, black in Fig. 1) with a maximum AMOC strength of 24.9 Sv and two freshwater forced runs with a maximum AMOC strength of close to zero (forced with 0.3 Sv freshwater input, called AMOC off, red in Fig. 1) and 10.2 Sv (forced with 0.2 Sv freshwater input, called AMOC weak, dark blue in Fig. 1), respectively to study the changes at different stadial to interstadial transitions. Our model setup is a very common one for studying millennial-scale glacial climate variability. Following the three mode conceptual model for D-O cycles (Alley et al. 1999; Rahmstorf 2002; Sarnthein et al. 2000) the assumption is that there are essentially three distinct ocean states, an interstadial/strong AMOC state, a non-Heinrich stadial state with a weak and shallow AMOC, and a Heinrich event state with a collapsed AMOC.

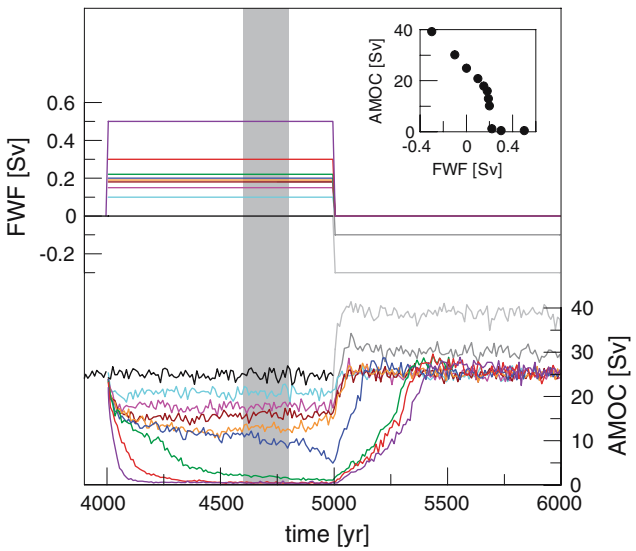

Fig. 1 Freshwater forcing (FWF) into the North Atlantic between 50°N and 70°N (*top*) and Atlantic meridional overturning circulation (AMOC, *bottom*). Amplitudes of the freshwater flux between model years 4,000 and 5,000 are 0.1, 0.15, 0.18, 0.19, 0.2, 0.22, and 0.3 Sv, respectively. Also shown are runs with −0.1 and −0.3 Sv freshwater forcing after model year 5,000 (*grey lines*). The averages of the 200 years *highlighted by the shaded area* are used in this study as quasi equilibrium states with different AMOC strength. The *inset figure shows* AMOC strength versus freshwater flux for the different quasi equilibrium states

However, the two different transitions used throughout this paper (AMOC off to AMOC strong and AMOC weak to AMOC strong) should be considered as exemplary cases. The model shows many different stable or quasi-stable (stable on timescales of several centuries) states of AMOC strength depending on the freshwater forcing applied to the North Atlantic (Fig. 1). Therefore, transitions between a range of states are conceivable, leading to a variety of different stadial to interstadial transitions. To explore the range of states a series of experiments were also simulated using negative freshwater perturbations starting from weak overturning states (examples shown as grey lines in Fig. 1). These simulations show similarly abrupt increases in the AMOC and warming patterns qualitatively consistent with the other transitions. However, the end states show a vigorous maximum AMOC of up to 40 Sv. These seem more and more unrealistic as the magnitude of the negative perturbation is increased, and are, therefore, not used throughout this paper. While a few models have shown the existence of a range of states and transitions (Schmittner et al. 2002), most less complex models tend to have only two or three states (e.g., Ganopolski and Rahmstorf (2002), Schulz et al. 2002), with usually more abrupt transitions in the less complex compared to the more comprehensive models (Rahmstorf et al. 2005).

Freshwater forcing is used here as a tool to obtain different AMOC states. We are interested only in the climate responses to the AMOC changes and do neither investigate the link between the absolute amount of freshwater forcing

and the corresponding AMOC state, nor study the cause for the different overturning strengths. We note that there are other mechanisms proposed as possible causes for changes in the AMOC including relaxation from an unstable/metastable state (Ganopolski and Rahmstorf 2002; Schmittner et al. 2002; Schulz et al. 2002), oscillatory behavior (Aeberhardt et al. 2000), noise induced transitions (Knutti and Stocker 2002), transitions induced by a very weak forcing (Ganopolski and Rahmstorf 2001), a combination of forcing and noise (Ganopolski and Rahmstorf 2002), slow changing boundary conditions (Wood et al. 1999) or spontaneous transitions due to internal variability (Goosse et al. 2002; Hall and Stouffer 2001; Sakai and Peltier 1997; Schaeffer et al. 2002; Schulz et al. 2007).

The work presented here focuses mainly on the seasonality of temperature differences between a strong AMOC state and states with a reduced or halted AMOC. A comprehensive model—data evaluation is not possible for the changes in seasonality due to the lack of paleo-data. Instead a comparison of monthly temperature and precipitation output of the preindustrial version of the model with reanalysis data is shown in Fig. 2 for different land regions of the northern hemisphere (see Table 1 for the definition of the regions). In general, the phasing of the seasonal cycle in temperature is well represented in the model. Temperatures are overestimated by up to a few degrees Celsius especially in the summer months in most regions. The quality of the representation of the phasing and the amplitude of the seasonal cycle in precipitation differs from region to region. But given the reduced complexity of the atmospheric model ECBILT, the representation is reasonably well.

Biases in the preindustrial seasonality of temperature and precipitation are likely to persist in our interstadial and stadial state model runs with LGM boundary conditions and freshwater perturbations, thus a substantial part of the biases will tend to cancel when comparing a particular season for different AMOC states. Therefore, we are more confident in the changes in seasonality than in the absolute values. This assumption is supported by the fact that in general, the patterns of change in different models (e.g., the future warming for higher CO_2 concentration) are more similar across models when differences are taken relative to the control state of each model than when considering absolute temperature predictions. However, we note also that the results for precipitation have to be interpreted with more caution than the temperature results.

3 Oceanic responses

Figure 3a, c and e show the AMOC patterns of the strong AMOC, the weak AMOC and the AMOC off state,

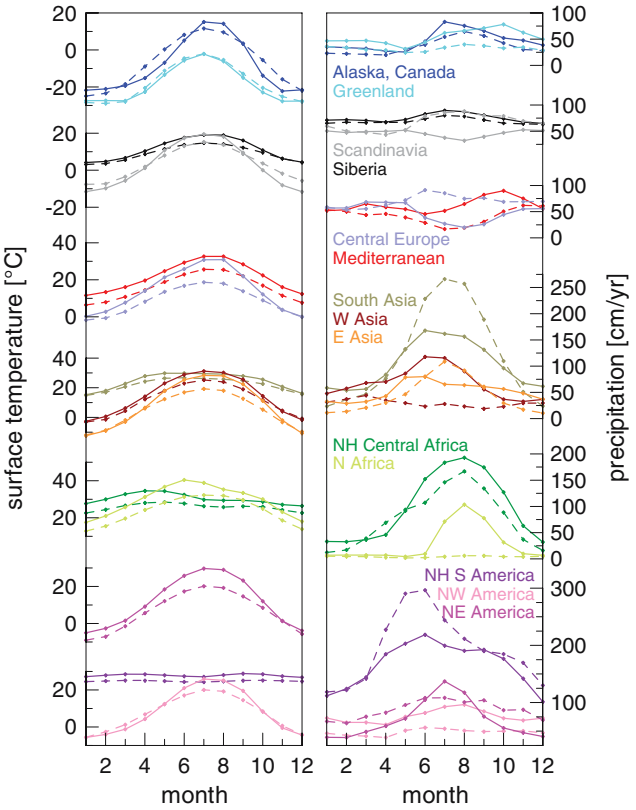

Fig. 2 Comparison of the modeled seasonal cycle for preindustrial boundary conditions (*solid lines*) in temperature (*left panel*) and precipitation (*right panel*) with observations (*dashed lines*) averaged over different regions of the northern hemisphere (definitions of the regions are given in Table 1). Modeled monthly temperatures are compared with ERA40 reanalysis data (Uppala et al. 2005), modeled monthly precipitation is compared with the CMAP precipitation data set (Xie and Arkin 1997)

Table 1 Definition of the different regions used in Figs. 2, 6, 8 and 9

Region	Longitude	Latitude
Alaska, North Canada	170–60°W	60–70°N
Greenland	60–20°W	60–85°N
Scandinavia	0–40°E	55–75°N
Central Europe	10–40°E	45–55°N
Mediterranean	10°W to 40°E	30–45°N
Siberia	40°E to 170°W	50–85°N
East Central Asia	80–140°E	30–50°N
West Central Asia	40–80°E	30–50°N
South Asia	60–130°E	10–30°N
North Africa	20°W to 40°E	20–30°N
NH Central Africa	30°W to 45°E	00–20°N
North West America	150–100°W	30–60°N
North East America	100–50°W	30–60°N
NH South America	90–20°W	00–15°N

A land mask is applied, and only values over land are used to calculate temperature and precipitation averages

respectively. The AMOC of the glacial control run (the strong AMOC state) shows a vigorous overturning cell, with North Atlantic deep water (NADW) formation reaching down to the bottom of the North Atlantic and maximum NADW export at 30°S of 17.1 Sv at a depth of 1,700 m. The weak AMOC state has a much weaker and slightly shallower maximum NADW export of 4.7 Sv at a depth of 1,200 m, while the off state does not show any substantial overturning and NADW export at all. The three different states exemplify an interstadial (strong AMOC), a non-Heinrich stadial (weak AMOC) and a Heinrich event (AMOC off).

The transition from an AMOC off/weak to a strong AMOC state leads to a large increase in the meridional heat transport. Heat is advected into the North Atlantic and the Nordic Seas where it is released to the atmosphere. The largest changes in the heat flux from the ocean to the atmosphere in these regions take place during the winter months due to a combination of two mechanisms. First, the temperature gradient between the ocean and the atmosphere is largest in winter, which leads to the large ocean to atmosphere heat release of the advected heat in the strong AMOC state. Second, the colder SST in winter compared to the other seasons lead to a deeper mixed layer and, therefore, the heat of a larger volume is mixed to the surface (Schmittner and Stocker 2001). In the AMOC off and AMOC weak states this mechanism is much weaker than in the strong AMOC state due to the freshwater forcing, which leads to a better stratified ocean and less deep mixing. Figure 3b shows the boreal winter surface heat flux from the ocean to the atmosphere of the strong AMOC state, Fig. 3d, f the change in winter ocean heat release for the weak AMOC to strong AMOC and the AMOC off to strong AMOC transition, respectively. The change in winter heat flux leads to the dominant winter surface air temperature warming in the North Atlantic region discussed in detail in Sect. 4. The transition from an AMOC off/weak to a strong AMOC state also leads to a significant sea ice retreat in the North Atlantic in all seasons, with the maximum change taking place in winter (Fig. 3d, f). In contrast to the heat flux, the increase in SST is similar for all months. The annual mean SST over the North Atlantic south of Iceland (50°W–20°E, 45°N–65°N) rises by 5.6 and 3.0°C for the AMOC off to strong AMOC and the AMOC weak to strong AMOC transition, respectively. Average SST increases in the Nordic Seas (35°W–20°E, 65°N–80°N) are 2.6 and 2.4°C, respectively.

4 Atmospheric responses

The simulated difference between the strong AMOC and the AMOC off/weak state shows a widespread warming in surface air temperature in most parts of the northern hemisphere. The warming shows large seasonal differences which are shown in Fig. 4 where summer and winter changes are compared for the two different transitions. The winter temperature increase is significantly larger in most parts of the northern hemisphere for both transitions. In the Arctic (north of the Arctic Circle) the winter transition on average is larger by a factor of 3.8 and 4.1 in the AMOC off to strong AMOC and the weak AMOC to strong AMOC transition, respectively. Along the northern coast of Alaska, in the Labrador Sea region, the Hudson Bay area and along the northern coast of Eurasia the ratio of winter to summer warming reaches up to a factor of 10 and more in regions where the summer temperature rise is particularly small. The largest absolute surface air temperature rises are centered in the Nordic Seas, where the ocean to atmosphere heat flux increases substantially in winter and the sea ice margin retreats and leads to open water in a large fraction of the Nordic Seas year round. The sea ice retreat is illustrated in Fig. 4 by the lines of 50% sea ice fraction, which we use as a measure for the sea ice margin for the different AMOC states and seasons. The retreat of the sea ice in the North Atlantic leads to a very pronounced decrease in the amplitude of the seasonal cycle in surface air temperature mainly over the regions where the winter sea ice disappears. Over these regions the amplitude of the seasonal cycle decreases on average by 76 and 66% for the AMOC off to strong AMOC and the AMOC weak to strong AMOC transition, respectively. Outside of the North Atlantic region, changes in the seasonal cycle are generally smaller than 30 and 15% in the off to strong AMOC and weak to strong AMOC transition, respectively.

The winter season shows the largest surface air temperature increase in the North Atlantic region and in most parts of the Arctic. This is, however, not the case for the whole northern hemisphere, an observation that will be discussed in more detail in this section. To illustrate the regional differences, Fig. 5 shows a map of the month with the largest and smallest temperature change, respectively, for the AMOC off to strong AMOC transition. The seasonal evolution of the temperature change for different land regions of the northern hemisphere is shown in Fig. 6 (for the definition of the different regions see Table 1). The month with the largest temperature increase is between November and February in the high northern latitudes, the North Atlantic, Scandinavia, Greenland, the Labrador Sea, Northern Canada and Alaska, in the Pacific north of 40°N, and the costal areas in northern Siberia. As discussed above, these regions are dominantly influenced by the changes in the North Atlantic, especially by the large increase in oceanic heat release to the atmosphere at high northern latitudes in winter. In the North Pacific the modeled sea ice retreat is responsible for the fact that the

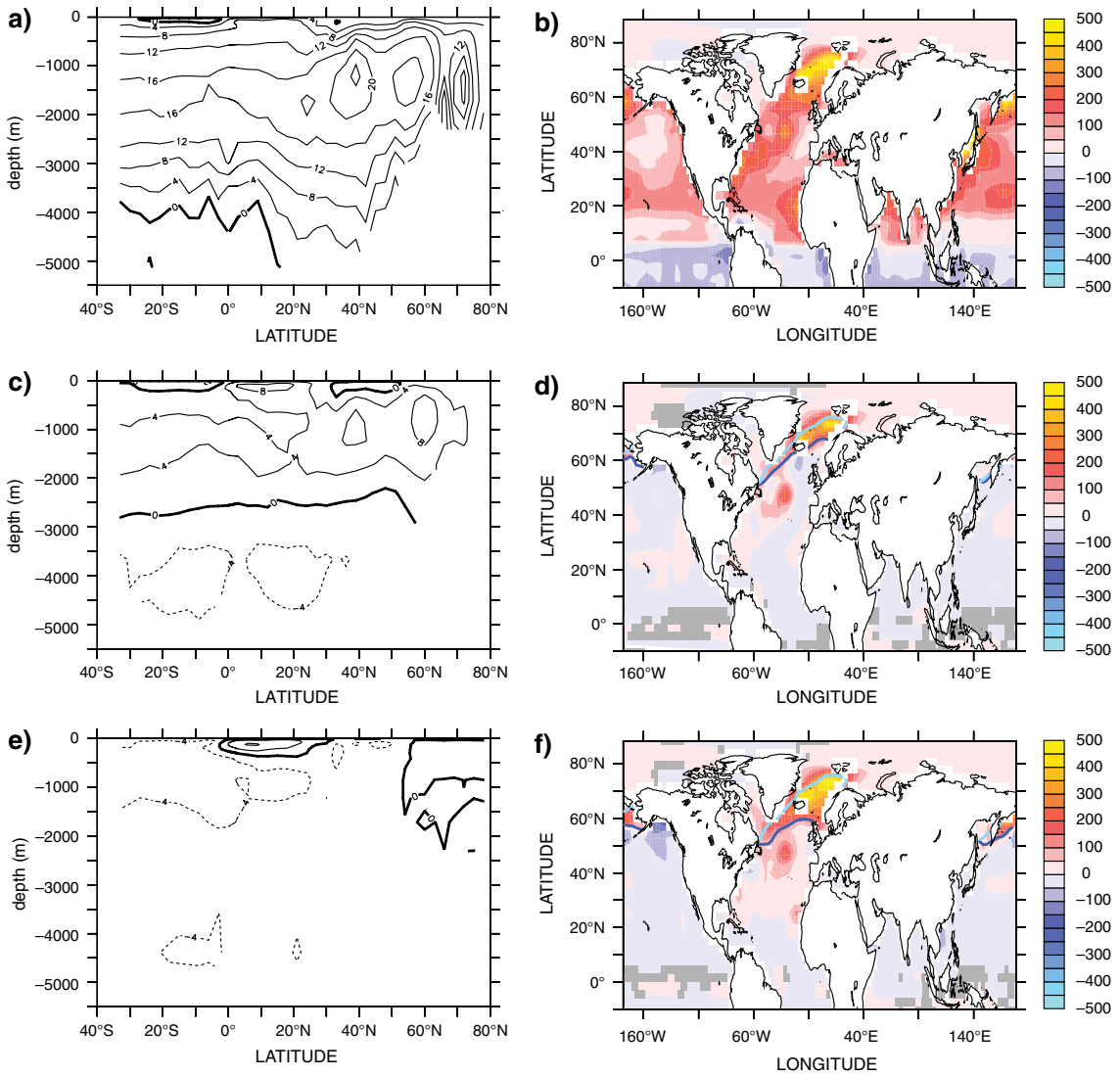

Fig. 3 Annual mean Atlantic meridional overturning stream function (Sv) for the strong AMOC (**a**), the weak AMOC (**c**), and the AMOC off states (**e**), respectively. *Solid lines* indicate clockwise, *dashed lines* counter clockwise currents. Contour spacing is 4 Sv. Winter (DJF) surface heat flux (Wm^{-2}) from the ocean to the atmosphere for the strong AMOC state (**b**), difference between the strong and the weak AMOC state (**d**) and difference between the strong AMOC and the AMOC off state (**f**), respectively. In **d** and **f,** *red colors* indicate an increase in heat flux from the ocean to the atmosphere, *blue colors* a decrease. Areas where the differences are not significant at the 95% level (compared to the noise in the 200 years averaging period) are shaded in *grey*. Overlaid are the modeled average winter sea ice margins for the strong AMOC (*cyan*), the weak AMOC (*dark blue*, **d**) and the AMOC off state (*dark blue*, **f**). The sea ice margin is defined as 50% sea ice cover

month with the largest temperature rise is between November and February. The land areas mentioned above are covered by ice sheets or snow year round in the AMOC off and the strong AMOC state. Other areas show snow free seasons in either the strong AMOC or in both states. Seasonal shifts in the snow cover and snow extent between the AMOC off and the strong AMOC state lead to a local amplification of the temperature change especially in spring. This is the case in large parts of Europe, northern Asia and along the west coast of North America between 40 and 55°N where an earlier onset of the snowmelt in spring leads to a strong positive snow-albedo feedback amplifying the temperature rise and leading to even larger temperature changes in spring than in winter. To illustrate this fact, the month with the largest albedo change is shown in Fig. 7. By how much the spring temperature increase is amplified depends on the local change in snow cover and snow extent. In Central Europe, for example, the changes are much larger than in the Mediterranean region, explaining the more pronounced spring warming.

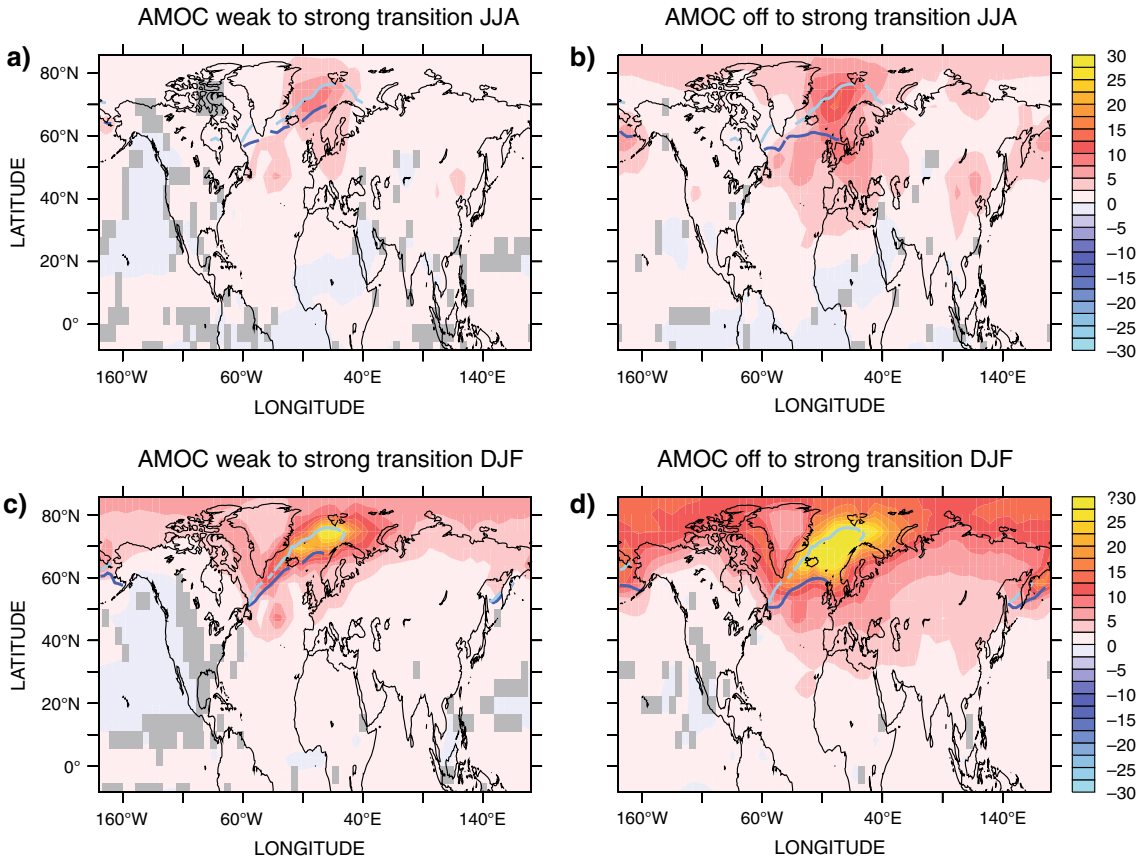

Fig. 4 **a** Modeled surface air temperature change (°C) for the transition AMOC weak to strong in summer (JJA) and **c** in winter (DJF) as well as **b** for the transition AMOC off to strong in summer (JJA) and **d** in winter (DJF). Areas where the differences are not significant at the 95% level (compared to the noise in the 200 years averaging period) are shaded in *grey*. Overlaid in each panel are the modeled average sea ice margins for the AMOC off/weak state (*dark blue*) and the strong AMOC state (*cyan*) for the corresponding transition and season

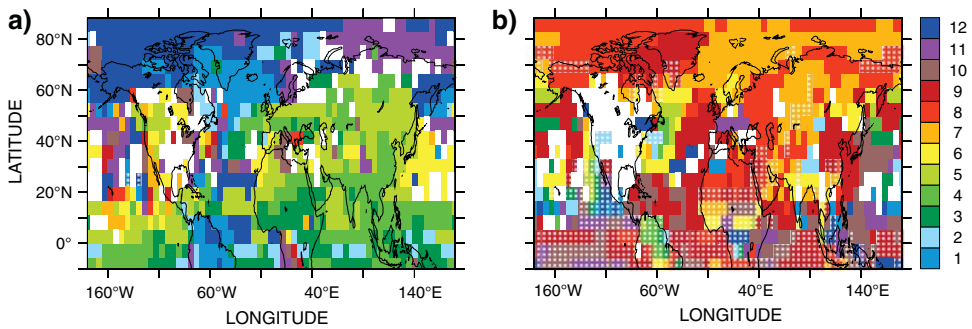

Fig. 5 Month of largest (**a**) and month of smallest surface air temperature change (**b**) for the AMOC off to strong AMOC transition. Areas where no single month is smallest or largest with a significance of 95% are shown in *white*. *White stippling* indicates that the temperature change is negative; *no stippling* means that the temperature change is positive. *Purple to blue colors* indicate November through February. *Green colors* are used for the northern hemisphere spring months. The northern hemisphere summer to early autumn months (June–September) are shown in *yellow* and *red colors*

The earlier decrease in snow cover and the related decrease in albedo in northern Eurasia lead to an earlier weakening and break down of the Siberian high pressure system (Kudrass et al. 2001; Meehl 1994). The Siberian high is responsible for the flow of relatively cold air with northeasterly winds to south eastern Asia and the Indian

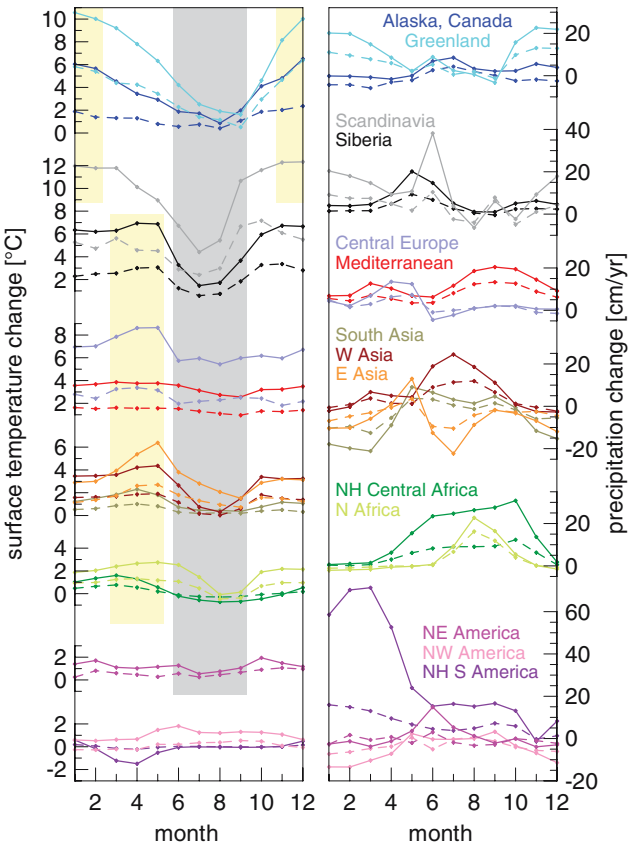

Fig. 6 Monthly temperature (*left panel*) and precipitation changes (*right panel*) for the AMOC off to strong AMOC transition (*solid lines*) as well as for the weak AMOC to strong AMOC transition (*dashed lines*), respectively. The definitions of the different regions are given in Table 1. For the AMOC off to strong AMOC transition the 3 months with the lowest temperature changes for all regions except western North America and northern hemispheric South America fall within the time period June through September. This is highlighted by the *gray shaded area*. The *yellow shaded areas* highlight the time periods with the 2–3 months showing the largest temperature rise. Two groups of regions stand out: the northern North Atlantic region and the high latitudes of North America, which show the largest temperature changes in November through February, and Eurasia/Africa, which undergo the largest temperature rises in March through May. The smallest and largest temperature changes take place during the same months for the weak AMOC to strong AMOC transition in most regions. See text for details

sub-continent. In southern Asia and the Indian sub-continent the earlier weakening of this flow in the strong AMOC state leads to a warming in spring in the AMOC off/weak to strong AMOC transition, which exceeds the temperature rise in winter. SST changes in the Indian Ocean are also largest in spring. This signal is transported westward by the trade winds and leads to larger temperature changes in spring compared to winter in the northern hemisphere part of Africa.

The North American continent south of 60°N shows only small temperature changes, the seasonal differences are less pronounced and it is not possible to define the

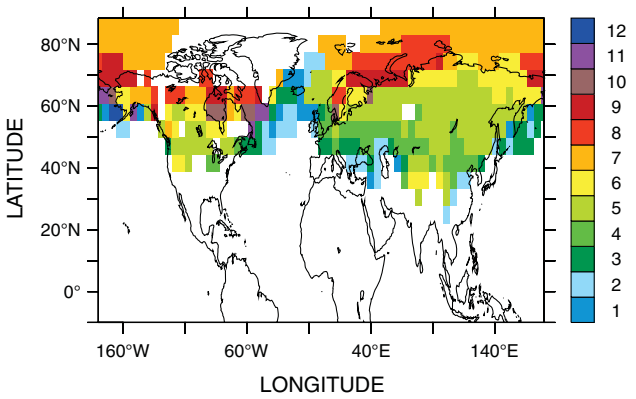

Fig. 7 Month of largest decrease in the albedo. Shown are areas with a decrease in albedo of 0.04 or more. The snow-albedo feedback is most important in Central Europe and Asia north of 50°N. The *green colors* in these areas indicate that the largest albedo decrease happens during the northern hemisphere spring months

month with the largest (smallest) temperature change with a significance level of 95% for many areas. The reason for the different response compared to Eurasia is the large Laurentide ice sheet reaching as far south as 40°N in the East, increasing the albedo by more than 60% in North America and dominating the local weather patterns and surface air temperatures (Peltier 1994; Timmermann et al. 2004). The northern hemispheric part of South America shows the largest temperature rise in December and January similar to Atlantic SST in these latitudes. The reason is that this region is influenced by the Northern Hemisphere warming signal in boreal winter, when the Intertropical Convergence Zone (ITCZ) is located further south.

The smallest temperature changes in the Arctic, over the North Atlantic and in most parts of the northern hemisphere over land, happen in summer to early autumn and minimum monthly temperature changes take place between June and September. South of 20°N the regions over land are also influenced by the changes in the southern hemisphere, i.e., showing a negative temperature response during these months in line with the bi-polar seesaw concept. Changes in the ITCZ further modify the pattern. This is for example the case in the northern hemisphere part of South America. The warmer temperatures in the northern hemisphere in the strong AMOC state lead to a northward shift of the ITCZ earlier in the year, causing a large increase in rainfall and an associated cooling signal in the northern part of South America. Therefore, the largest temperature decrease in this region takes place in March and April. The largest temperature decreases in Africa between 0 and 20°N take place in summer and are also related to the largest increases in local rainfall. The seasonal timing of the lowest surface air temperature changes over the Pacific shows large regional differences and no clear structure mainly due to the small overall temperature

change and no clear seasonality in the temperature change. In general, the extreme changes of surface air temperature away from the sea ice edges take place in the same month as when the SST change is largest/smallest.

A detailed evaluation of the model findings discussed above with paleo-data is difficult, since monthly or even seasonal paleo-proxy records for temperature do not exist for most regions. Two exceptions are Greenland and Europe. For Greenland, there is clear evidence that temperature changes in winter were much larger than in summer. Available data cover the Younger Dryas cold event (YD). Reconstructions from δ^{15}N measured on N_2 in the air trapped in the GISP2 ice core show that the annual mean temperature was 15°C lower during the YD compared to the early Holocene (Severinghaus et al. 1998). The estimates for the January and July temperature decrease based on glacier evidence from eastern Greenland range from 20 to 25°C and 5 to 10°C, respectively (Denton et al. 2005; Lie and Paasche 2006). According to these data the July–January difference was 10–20°C larger during the YD cold phase than during the early Holocene. The temperature rise at the termination of the YD is one of the larger reconstructed annual mean temperature changes and, therefore, probably gives an upper limit of the expected seasonal changes. δ^{15}N measurements for a series of D-O events show a range of the annual mean temperature change of 8–16°C (Huber et al. 2006; Landais et al. 2004). Our model results show an average Greenland annual mean temperature rise for an AMOC off to strong AMOC transition of 6.4°C, slightly underestimating the lower bound of the reconstructed temperature changes. The modeled January and July temperature increases are 10.6 and 2.5°C, respectively, the July–January difference is 8.1°C larger during the cold AMOC off state than during the warm strong AMOC state. Overall, our model results agree at least qualitatively with the paleo-data evidence from Greenland. January and July temperature change reconstructions are also available for Europe based on geological and palaeoecological data (Renssen and Isarin 2001) for the onset of the Bølling-Allerød and the termination of the YD. The model results underestimate the temperature rise in winter as in the case of Greenland but overestimate it in summer. No temperature reconstructions are available for the spring season to test our model result that largest temperature changes in Europe take place in spring.

The magnitude of the modeled temperature change is significantly larger for the AMOC off to strong AMOC transition than for the weak AMOC to strong AMOC transition. This is expected from the difference in the AMOC strengthening. However, Fig 8 shows that the temperature changes of the two transitions do not scale linearly with respect to the change in meridional heat transport or AMOC and show large regional and seasonal

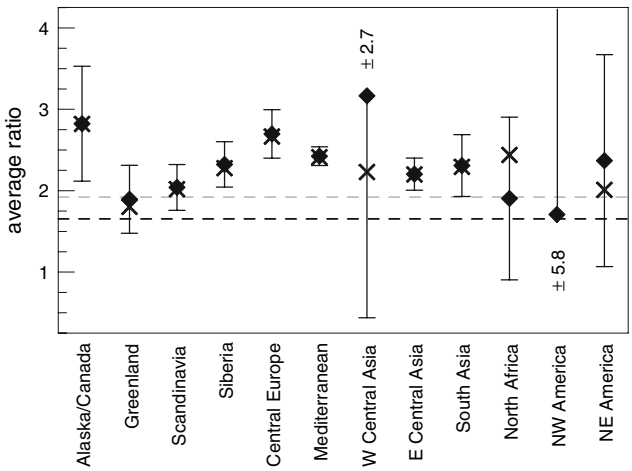

Fig. 8 Ratios of the AMOC off to strong AMOC and the weak AMOC to strong AMOC temperature changes for different regions (see Table 1 for the definition of the regions). Shown are the average (*diamonds*) and the one sigma standard deviation (*error bar*) of the 12 monthly temperature change ratios as well as the ratio of the annual mean temperature changes (*crosses*). Also shown are the ratios of the Atlantic meridional heat transport at 25°N (*grey dashed line*) and the maximum AMOC (*black dashed line*). The scatter of the average ratios indicates spatial differences; the *error bar* for each region highlights seasonal differences between the two transitions

differences in their ratio. The average ratio over all months of the AMOC off to strong AMOC versus the weak AMOC to strong AMOC transition for the regions shown in Fig. 6 (apart from northern hemispheric South America, which shows a negative ratio) ranges from 1.7 to 3.2, meaning that the AMOC off to strong AMOC transition is larger by a factor of 1.7–3.2 than the weak AMOC to strong AMOC transition. For comparison, the ratio of the AMOC strengthening is 1.7 and that of the Atlantic meridional heat transport changes at 25°N is 1.9. The seasonal variation in the temperature ratio in certain regions can be even larger than the spatial differences, and reaches a standard deviation of up to 5.8 in western North America. Reasons for the regional and seasonal differences in the ratio are the different extent of the two discussed transitions as well as regional and seasonal non-linear feedback mechanisms influencing the local temperature response. The implications of these findings on the interpretation of paleoclimate proxy data are discussed in Sect. 5.

The seasonality of the precipitation changes for the AMOC off to strong AMOC and the weak AMOC to strong AMOC transition shows a much less homogenous picture because of the more local nature of precipitation and the regional changes in precipitation patterns. Large seasonal and regional differences are observed and the sign of the precipitation change in many of the regions depends on the season (Fig. 6). In Greenland, for example, the model predicts an annual mean increase in precipitation of 0.11 m year^{-1}, in agreement with the reconstructed

increase in the accumulation rate over D-O events of about 0.10 m year^{-1} (Alley et al. 1993; Wagner et al. 2001). The largest increase in precipitation is found during November through February, while the changes in May through September are small. This is in agreement with the fact that δ^{18}O records measured on the ice of Greenland ice cores underestimate the temperature changes of D-O events if the relation between δ^{18}O and temperature is derived from today's spatial pattern (Jouzel 1999). The relative contribution of winter snow is smaller during stadials than during interstadials leading to biases towards too high reconstructed annual mean temperatures during stadials. This effect is additionally amplified by the fact that the cold anomaly during the stadial states is most pronounced in winter. West and South Asia show increased precipitation during the summer months, which is consistent with paleodata showing stronger monsoon during interstadials (Schulz et al. 1998; Wang et al. 2001). The largest precipitation increase is modeled in the northern hemisphere part of South America between January and April as a result of the ITCZ being shifted further to the north in those months in the strong AMOC state. However, tropical precipitation patterns in the ECBILT-CLIO model should be interpreted with some caution. Due to the simplifications in the dynamical equations and the limited vertical resolution, the atmospheric dynamics near the equator are not well simulated.

Each of the seasonal temperature and precipitation change curves shown in Fig. 6 represents the average over a region that covers a number of model grid points. The question arises whether the average curves represent the changes in these regions in an adequate way and how much variability exists in the model on sub-regional scale. Figure 9 shows the average temperature and precipitation changes and one standard deviation of all the grid points in that region for the AMOC off to strong AMOC transition for Greenland, Central Europe and South Asia. The spread is caused by spatial differences in the response pattern. The effect of temporal noise (i.e., interannual variability) is negligibly small, since the change at each grid point is a difference between two periods that are each averaged over 200 years. The spread in the precipitation change in general is much larger than in the temperature change, highlighting the more local characteristics of precipitation and changes in precipitation patterns. The largest spread in temperature is found in Greenland as well as in Scandinavia (not shown). This is due to the latitudinal differences especially in the sea ice retreat. Large winter temperature increases are found at southern locations, close to areas with large winter sea ice changes over the stadial to interstadial transition. Winter changes decrease to the north and get smaller the farther the location is from the sea ice edge. Summer changes are smallest in the south and

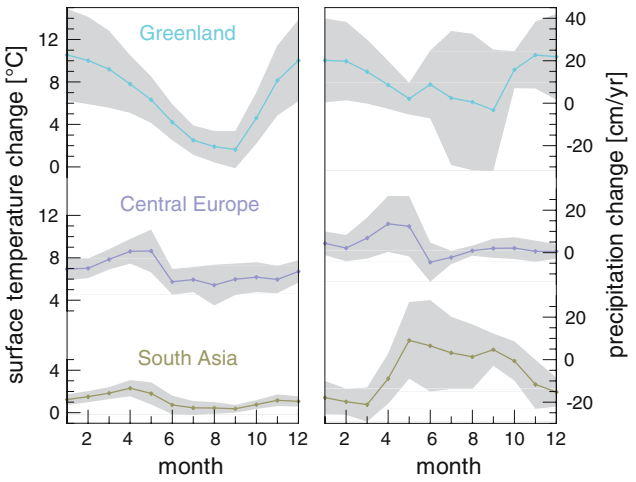

Fig. 9 Examples of the scatter in temperature (*left panel*) and precipitation changes (*right panel*) within three different regions over an AMOC off to strong AMOC transition in each month: Greenland (*top*), Central Europe (*middle*), and South Asia (*bottom*). *Solid lines* denote the average (as in Fig. 6), *shaded areas* the plus, minus one standard deviation range of temperature and precipitation changes, respectively over the *grid boxes* belonging to the region. The definitions of the regions are given in Table 1

increase towards the north due to the different location of the summer sea ice edge. This implies that in Greenland and in Scandinavia the further one goes north, the less extreme are the seasonal differences in the temperature change.

All results presented here use LGM boundary conditions for greenhouse gas concentrations, orbital parameters, topography on land and albedo. However, many parameters of the climate system changed over the last glacial period and probably modulated the amplitude and spatial patterns of the temperature and precipitation changes at the onset of D-O events. The size of the Laurentide and the Fennoscandinavian ice sheets, for example, was significantly smaller during marine isotope stage (MIS) 3 than during the LGM (Marshall and Clarke 1999; Zweck and Huybrechts 2005). The ice sheet size has a significant impact on regional atmospheric circulations, temperature and precipitation and it is possible that the temperature rise at the onset of D-O events in North America was larger during MIS 3 than in our LGM model simulations. Therefore, our modeled temperature and precipitation changes should be interpreted as qualitative rather than quantitative results.

5 Implications for paleo-records

Several model results discussed in the earlier sections of this paper have important implications for the interpretation of paleo-records from different archives and locations. Model results, for example, highlight that the response to a

change in the AMOC differs substantially between different seasons. Further, not all regions and climate parameters show the same seasonal characteristics in their response. Most paleo-proxies record seasonal rather than annual mean climate conditions and are often influenced by more than just one climate parameter (e.g., temperature and precipitation). Based on our findings they cannot be used as annual mean climate change reconstructions without correcting for seasonal biases. Rather they should be used as seasonal indicators. Different proxies recording different seasons are desirable for each location to reconstruct and better understand the seasonal patterns of D-O events.

The model results presented here focus on two exemplary transitions (AMOC off to strong AMOC versus weak AMOC to strong AMOC). They show differences in the amplitude, the seasonal pattern and the spatial extent of the anomalies (e.g., in temperature) observed in the northern hemisphere. Based on the model simulations shown in Fig. 1, transitions between other AMOC states are possible as well leading to a variety of different transitions with slightly different flavors. This highlights the importance of local feedback mechanisms such as, for example, snow-albedo feedbacks or shifts in sea ice margins. In the case of sea ice, the retreat of a sea ice margin can dominate a climate variable at a certain location in one transition, while in another transition the sea ice retreat takes place further away and the same climate variable at the same location undergoes much smaller changes. All these findings help to explain why paleo-records from many different regions show variable amplitudes for different D-O events (Flückiger et al. 2004; Genty et al. 2003; Hendy and Kennett 2003; Huber et al. 2006; Ortiz et al. 2004; Schulz et al. 1998; Shackleton et al. 2000; Wang et al. 2001; Zic et al. 2002) or even lack some of the D-O events (Peterson et al. 2000). On the other hand this means that conclusions from a single D-O event cannot necessarily be transferred quantitatively to other events. Therefore, it is desirable to get a high spatial coverage of well-resolved and well dated paleo-records to study the variability between different stadial and interstadial events.

6 Conclusions

ECBILT-CLIO results show that a shift to a stronger AMOC leads to a widespread temperature increase in the northern hemisphere. The seasonality of the temperature rise shows large regional differences. While the largest changes take place in November through February in high northern latitudes and in the North Atlantic region north of 55°N, the largest temperature increases in most other land regions are seen in spring. Smallest temperature changes are observed in June through September in most of the northern hemisphere land regions. The dominant winter signal at high northern latitudes and in the North Atlantic is due to the strong seasonality of the oceanic heat release. The ocean to atmosphere heat flux peaks during the winter months and the retreat of the sea ice during winter allows interaction of the ocean and the atmosphere on a large scale, leading to the dominant winter warming in this region. Further away other factors influence the seasonal distribution of the temperature rise. An earlier snowmelt and the associated change in albedo lead to the largest temperature increase in April and May in Europe and northern Asia. This signal is propagated to the southern parts of Asia through an earlier breakdown of the Siberian high pressure system and the related decrease in the advection of cold air to the south. Temperature changes during an AMOC off/weak to a strong AMOC transition in North America south of 60°N are generally small due to the large extent of the Laurentide ice sheet, which dominates the climate and smoothes out temperature changes. Precipitation changes at the onset of an interstadial are much less homogenous because of the more local nature of precipitation and the regional changes in precipitation patterns.

The temperature and precipitation change patterns for different changes in the AMOC are not linear. Local non-linearities (such as for example the local retreat of sea ice) influence the amplitude of the annual mean response as well as the response in different seasons. This finding together with the fact that models like ECBILT-CLIO show different equilibrium states (in this study depending on the freshwater forcing) leads to the conclusion that a variety of realizations for a stadial to interstadial transition is possible. This can explain the fact that paleo-records from various locations show different amplitudes for different D-O events and that the amplitudes can be different for each region and season.

Given the complexity of the signal of abrupt climate events even in this simplified model, we suggest that proxy records of environmental change, which are additionally affected by local processes like surface interactions or land cover not discussed here, may tell a complicated story of past climate change. Inferring amplitudes, extents and large-scale characteristics of abrupt climate events from proxies and interpreting connections between different proxy locations might not be as straightforward as often assumed.

Acknowledgments We are grateful to the model developers for making ECBILT-CLIO available to the scientific community and thank three anonymous reviewers for their comments, which have helped to improve the manuscript. JF was supported by NSF award OPP ARC0519512, by INSTAAR, University of Colorado at Boulder, USA, and ETH Zurich, Switzerland. RK was supported by the Swiss National Science Foundation, NCAR, and ETH Zurich. NCAR is sponsored by the National Science Foundation.

References

Aeberhardt M, Blatter M, Stocker TF (2000) Variability on the century time scale and regime changes in a stochastically forced, zonally-averaged ocean–atmosphere model. Geophys Res Lett 27:1303–1306

Alley RB, Clark PU, Keigwin LD, Webb RS (1999) Making sense of millennial-scale climate change. In: Clark PU, Webb RS, Keigwin LD (eds) Mechanisms of global climate change at millennial time scales, vol 112. AGU, Washington, pp 385–394

Alley RB, Meese DA, Shuman CA, Gow AJ, Taylor KC, Grootes PM, White JWC, Ram M, Waddington ED, Mayewski PA, Zielinski ZA (1993) Abrupt increase in Greenland snow accumulation at the end of the Younger Dryas event. Nature 362:527–529

Collins WD, Bitz CM, Blackmon ML, Bonan GB, Bretherton CS, Carton JA, Chang P, Doney SC, Hack JJ, Henderson TB, Kiehl JT, Large WG, McKenna DS, Santer BD, Smith RD (2006) The community climate system model version 3 (CCSM3). J Clim: 2122–2143

Curry WB, Oppo DW (1997) Synchronous, high-frequency oscillations in tropical sea surface temperatures and North Atlantic deep water production during the last glacial cycle. Paleoceanography 12(1):1–14

Dansgaard W, Johnsen SJ, Clausen HB, Dahl-Jensen D, Gundestrup NS, Hammer CU, Hvidberg CS, Steffensen JP, Sveinbjörnsdottir AE, Jouzel J, Bond G (1993) Evidence for general instability of past climate from a 250 kyr ice-core record. Nature 364:218–220

Denton GH, Alley RB, Comer GC, Broecker WS (2005) The role of seasonality in abrupt climate change. Quat Sci Rev 24(10–11):1159–1182

Elliot M, Labeyrie L, Duplessy J-C (2002) Changes in North Atlantic deep-water formation associated with the Dansgaard-Oeschger temperature oscillations (60–10 ka). Quat Sci Rev 21(10):1153–1165

Fawcett PJ, Agustsdottir AM, Alley RB, Shuman CA (1997) The Younger Dryas termination and North Atlantic deepwater formation: insights from climate model simulations and Greenland ice core data. Paleoceanography 12(1):23–38

Flückiger J, Blunier T, Stauffer B, Chappellaz J, Spahni R, Kawamura K, Schwander J, Stocker TF, Dahl-Jensen D (2004) N_2O and CH_4 variations during the last glacial epoch: insight into global processes. Glob Biogeochem Cycles 18:GB1020. doi:1010.1029/2003GB002122

Flückiger J, Knutti R, White JWC (2006) Oceanic processes as potential trigger and amplifying mechanisms for Heinrich events. Paleoceanography 21:PA2014. doi:2010.1029/2005PA001204

Ganopolski A, Rahmstorf S (2001) Rapid changes of glacial climate simulated in a coupled climate model. Nature 409:153–158

Ganopolski A, Rahmstorf S (2002) Abrupt glacial climate changes due to stochastic resonance. Phys Rev Lett 88(3):038501

Genty D, Blamart D, Ouahdi R, Gilmour M, Baker A, Jouzel J, Van-Exter S (2003) Precise dating of Dansgaard-Oeschger climate oscillations in western Europe from stalagmite data. Nature 421:833–837

Goosse H, Fichefet T (1999) Importance of ice–ocean interactions for the global ocean circulation: a model study. J Geophys Res 104(C10):23337–323355

Goosse H, Renssen H, Selten FM, Haarsma RJ, Opsteegh JD (2002) Potential causes of abrupt climate events: a numerical study with a three-dimensional climate model. Geophys Res Lett 29(18):1860. doi:1810.1029/2002GL014993

Hall A, Stouffer J (2001) An abrupt climate event in a coupled ocean-atmosphere simulation without external forcing. Nature 409:171–174

Hendy IL, Kennett JP (2003) Tropical forcing of North Pacific intermediate water distribution during Late Quaternary rapid climate change? Quat Sci Rev 22:673–689

Huber C, Leuenberger M, Spahni R, Flückiger J, Schwander J, Stocker TF, Johnsen S, Landais A, Jouzel J (2006) Isotope calibrated Greenland temperature record over Marine Isotope Stage 3 and its relation to CH_4. Earth Planet Sci Lett 243(3–4):504–519

Ji J, Chen J, Balsam W, Lu H, Sun Y, Xu H (2004) High resolution hematite/goethite records from Chinese loess sequences for the last glacial–interglacial cycle: rapid climatic response of the East Asian monsoon to the tropical Pacific. Geophys Res Lett 31:L03207. doi:03210.01029/02003GL018975

Jouzel J (1999) Calibrating the isotopic paleothermometer. Science 286:910–911

Knutti R, Flückiger J, Stocker TF, Timmermann A (2004) Strong hemispheric coupling of glacial climate through freshwater discharge. Nature 430:851–856

Knutti R, Stocker TF (2002) Limited predictability of the future thermohaline circulation close to an instability threshold. J Clim 15:179–186

Kudrass HR, Hofmann A, Doose H, Emeis K, Erlenkeuser H (2001) Modulation and amplification of climatic changes in the Northern Hemisphere by the Indian summer monsoon during the past 80 k years. Geology 29(1):63–66

Landais A, Barnola J-M, Masson-Delmotte V, Jouzel J, Chappellaz J, Caillon N, Huber C, Leuenberger M, Johnsen SJ (2004) A continuous record of temperature evolution over a sequence of Dansgaard-Oeschger events during Marine Isotopic Stage 4 (76–62 k years BP). Geophys Res Lett 31:L22211. doi:22210.21029/22004GL021193

Lang C, Leuenberger M, Schwander J, Johnsen S (1999) 16°C rapid temperature variation in central Greenland 70,000 years ago. Science 286:934–937

Li C, Battisti DS, Schrag DP, Tziperman E (2005) Abrupt climate shifts in Greenland due to displacements of the sea ice edge. Geophys Res Lett 32:L19702. doi:19710.11029/12005GL023492

Lie Ø, Paasche Ø (2006) How extreme was northern hemisphere seasonality during the Younger Dryas? Quat Sci Rev 25(5–6):404–407

Lynch-Stieglitz J, Adkins JF, Curry WB, Dokken T, Hall IR, Herguera JC, Hirschi JJ-M, Ivanova EV, Kissel C, Marchal O, Marchitto TM, McCave IN, McManus JF, Mulitza S, Ninnemann U, Peeters F, Yu E-F, Zahn R (2007) Atlantic meridional overturning circulation during the Last Glacial Maximum. Science 316:66–69

Marchal O, Stocker TF, Joos F (1998) Impact of oceanic reorganizations on the ocean carbon cycle and atmospheric carbon dioxide content. Paleoceanography 13(3):225–244

Marshall SJ, Clarke GKC (1999) Modeling North American freshwater runoff through the last glacial cycle. Quat Res 52(3):300–315

McManus JF, Francois R, Gherardi J-M, Keigwin LD, Brown-Leger S (2004) Collapse and rapid resumption of Atlantic meridional circulation linked to deglacial climate changes. Nature 428:834–837

Meehl GA (1994) Coupled land–ocean–atmosphere processes and South Asian monsoon variability. Science 266:263–267

Müller UC, Pross J, Bibus E (2003) Vegetation response to rapid climate change in Central Europe during the past 140,000 year based on evidence from the Füramoos pollen record. Quat Res 59:235–245

North Greenland Ice Core Project members (2004) High-resolution record of Northern Hemisphere climate extending into the last interglacial period. Nature 431:147–151

Opsteegh JD, Haarsma RJ, Selten FM, Kattenberg A (1998) ECBILT: a dynamic alternative to mixed boundary conditions in ocean models. Tellus 50A:348–367

Ortiz JD, O'Connell SB, DelViscio J, Dean W, Carriquiry JD, Marchitto T, Zheng Y, van Geen A (2004) Enhanced marine productivity off western North America during warm climate intervals of the past 52 k years. Geology 32(6):521–524

Peltier WR (1994) Ice age paleotopography. Science 265:195–201

Peterson LC, Haug GH, Hughen KA, Röhl U (2000) Rapid changes in the hydrologic cycle of the tropical Atlantic during the last glacial. Science 290:1947–1951

Rahmstorf S (2002) Ocean circulation and climate during the past 120,000 years. Nature 419:207–214

Rahmstorf S, Crucifix M, Ganopolski A, Goosse H, Kamenkovich I, Knutti R, Lohmann G, Marsh R, Mysak LA, Wang Z, Weaver AJ (2005) Thermohaline circulation hysteresis: a model intercomparison. Geophys Res Lett 32(23):L23605. doi:23610.21029/22005GL023655

Renssen H, Bogaart PW (2003) Atmospheric variability over the ~14.7 k years BP stadial–interstadial transition in the North Atlantic region as simulated by an AGCM. Clim Dyn 20(2–3):301–313

Renssen H, Isarin RFB (2001) The two major warming phases of the last deglaciation at ~14.7 and ~11.5 ka cal BP in Europe: climate reconstructions and AGCM experiments. Glob Planet Change 30(1–2):117–153

Roche DM, Dokken TM, Goosse H, Renssen H, Weber SL (2007) Climate of the Last Glacial Maximum: sensitivity studies and model-data comparison with the LOVECLIM coupled model. Clim Past 3:205–224

Sakai K, Peltier WR (1997) Dansgaard–Oeschger oscillations in a coupled atmosphere–ocean climate model. J Clim 10(5):949–970

Sarnthein M, Stattegger K, Dreger D, Erlenkeuser H, Grootes P, Haupt BJ, Jung S, Kiefer T, Kuhnt W, Pflaumann U, Schäfer-Neth C, Schulz H, Schulz M, Seidov D, Simstich J, van Kreveld S, Vogelsang E, Völker A, Weinelt M (2000) Fundamental modes and abrupt changes in North Atlantic circulation and climate over the last 60 k years—concepts, reconstruction and numerical modeling. In: Schäfer P, Ritzrau W, Schlüter M, Thiede J (eds) The northern North Atlantic: a changing environment. Springer, Berlin, pp 365–410

Schaeffer M, Selten FM, Opsteegh JD, Goosse H (2002) Intrinsic limits to predictability of abrupt regional climate change in IPCC SRES scenarios. Geophys Res Lett 29(16):1767. doi:1710.1029/2002GL015254

Schmittner A, Saenko OA, Weaver AJ (2003) Coupling of the hemispheres in observations and simulations of glacial climate change. Quat Sci Rev 22:659–671

Schmittner A, Stocker TF (2001) A seasonally forced ocean–atmosphere model for paleoclimate studies. J Clim 14:1055–1068

Schmittner A, Yoshimori M, Weaver AJ (2002) Instability of glacial climate in a model of the ocean–atmosphere–cryosphere system. Science 295:1489–1493

Schulz H, von Rad U, Erlenkeuser H (1998) Correlation between Arabian Sea and Greenland climate oscillations of the past 110,000 years. Nature 393:54–57

Schulz M, Paul A, Timmermann A (2002) Relaxation oscillators in concert: a framework for climate change at millennial timescales during the late Pleistocene. Geophys Res Lett 29(24):2193. doi:2110.1029/2002GL016144

Schulz M, Prange M, Klocker A (2007) Low-frequency oscillations of the Atlantic Ocean meridional overturning circulation in a coupled climate model. Clim Past 3:97–107

Severinghaus JP, Sowers T, Brook EJ, Alley RB, Bender ML (1998) Timing of abrupt climate change at the end of the Younger Dryas interval from thermally fractionated gases in polar ice. Nature 391:141–146

Shackleton NJ, Hall MA, Vincent E (2000) Phase relationships between millennial scale events 64,000 to 24,000 years ago. Paleoceanography 15(6):565–569

Spötl C, Mangini A (2002) Stalagmite from the Austrian Alps reveals Dansgaard-Oeschger events during isotope stage 3: implications for the absolute chronology of Greenland ice cores. Earth Planet Sci Lett 203:507–518

Stocker TF, Marchal O (2000) Abrupt climate change in the computer: is it real? Proc US Natl Acad Sci 97(4):1362–1365

Timmermann A, Justino FB, Jin F-F, Goosse H (2004) Surface temperature control in the North and tropical Pacific during the last glacial maximum. Clim Dyn 23(3–4):353–370

Timmermann A, Krebs U, Justino F, Goosse H, Ivanochko T (2005) Mechanisms for millennial-scale global synchronization during the last glacial period. Paleoceanography 20:PA4008. doi:4010.1029/2004PA001090

Uppala SM, Kållberg PW, Simmons AJ, Andrae U, da Costa Bechtold V, Fiorino M, Gibson JK, Haseler J, Hernandez A, Kelly GA, Li X, Onogi K, Saarinen S, Sokka N, Allan RP, Andersson E, Arpe K, Balmaseda MA, Beljaars ACM, van de Berg L, Bidlot J, Bormann N, Caires S, Chevallier F, Dethof A, Dragosavac M, Fisher M, Fuentes M, Hagemann S, Hólm E, Hoskins BJ, Isaksen L, Janssen PAEM, Jenne R, McNally AP, Mahfouf J-F, Morcrette J-J, Rayner NA, Saunders RW, Simon P, Sterl A, Trenberth KE, Untch A, Vasiljevic D, Viterbo P, Woollen J (2005) The ERA-40 re-analysis. Quart J R Meteorol Soc 131:2961–3012

Voelker AHL, workshop participants (2002) Global distribution of centennial-scale records for Marine Isotope Stage (MIS) 3: a database. Quat Sci Rev 21(10):1185–1212

Wagner G, Laj C, Beer J, Kissel C, Muscheler R, Masarik J, Synal H-A (2001) Reconstruction of the paleoaccumulation rate of central Greenland during the last 75 k years using the cosmogenic radionuclides ^{36}Cl and ^{10}Be and geomagnetic field intensity data. Earth Planet Sci Lett 193:515–521

Wang YJ, Cheng H, Edwards RL, An ZS, Wu JY, Shen C-C, Dorale JA (2001) A high-resolution absolute-dated late Pleistocene monsoon record from Hulu Cave, China. Science 294:2345–2348

Weber SL, Drijfhout SS, Abe-Ouchi A, Crucifix M, Eby M, Ganopolski A, Murakami S, Otto-Bliesner B, Peltier WR (2007) The modern and glacial overturning circulation in the Atlantic ocean in PMIP coupled model simulations. Clim Past 3:51–64

Wood RA, Keen AB, Mitchell JFB, Gregory JM (1999) Changing spatial structure of the thermohaline circulation in response to atmospheric CO_2 forcing in a climate model. Nature 399:572–575

Xie PP, Arkin PA (1997) Global precipitation: a 17-year monthly analysis based on gauge observations, satellite estimates, and numerical model outputs. Bull Am Meteorol Soc 78(11):2539–2558

Zic M, Negrini RM, Wigand PE (2002) Evidence of synchronous climate change across the northern hemisphere between the north Atlantic and the northwestern Great Basin, United States. Geology 30(7):635–638

Zweck C, Huybrechts P (2005) Modeling of the northern hemisphere ice sheets during the last glacial cycle and glaciological sensitivity. J Geophys Res 110:D07103. doi:07110.01029/02004JD005489